Environ. Sci. Technol. **2004**, *38,* 6074−6077

Arsenic Sequestration by Ferric Iron Plaque on Cattail Roots

NICOLE KEON BLUTE,*,†,‡
DANIEL J. BRABANDER,†,§
HAROLD F. HEMOND,†
STEPHEN R. SUTTON,||,⊥
MATTHEW G. NEWVILLE,|| AND
MARK L. RIVERS||,⊥

Ralph M. Parsons Laboratory, Department of Civil and Environmental Engineering, Massachusetts Institute of Technology, Cambridge, Massachusetts 02139, and Consortium for Advanced Radiation Sources and Department of Geophysical Sciences, University of Chicago, Chicago, Illinois 60637

Typha latifolia (cattail) sequesters arsenic within predominantly ferric iron root coatings, thus decreasing mobility of this toxic element in wetland sediments. Element-specific XRF microtomographic imaging illustrated a high spatial correlation between iron and arsenic in root plaques, with little arsenic in the interior of the roots. XANES analyses demonstrated that the plaque was predominantly ferric iron and contained approximately 20% As(III) and 80% As(V), which is significant because the two oxidation states form species that differ in toxicity and mobility. For the first time, spatial distribution maps of As oxidation states were developed, indicating that As(III) and As(V) are both fairly heterogeneous throughout the plaque. Chemical extractions showed that As was strongly adsorbed in the plaque rather than coprecipitated. Iron and arsenic concentrations ranged from 0.03 to 0.8 g Fe g^{-1} wet plaque and 30 to 1200 μg As g^{-1} wet plaque, consistent with a mechanism of As adsorption onto Fe(III) oxyhydroxide plaque. Because this mechanism decreases the concentrations of both As(III) and As(V) in groundwater, we propose that disruption of vegetation could increase the concentrations of mobile arsenic.

Introduction

The USEPA recently reduced the drinking water standard for arsenic (As) from 50 μg L^{-1} to 10 μg L^{-1} to reduce risks to public health. Concern for drinking water safety encourages research into processes that affect the mobility of As in the environment (*1*−*4*)—processes that are invariably dependent on speciation of both As and any solid phases with which As may adsorb or coprecipitate. Redox conditions strongly impact the aqueous and solid phase distribution of inorganic As species. Arsenic mobility is typically highest under iron-reducing, low-sulfide conditions in which As(III) is the predominant species (*5*); such conditions can be produced in freshwater wetlands by microbial respiration of organic matter together with impeded oxygen diffusion through waterlogged sediment pores (*6*).

Wetland plant roots, however, can oxidize the root environment (rhizosphere) in the immediate proximity (tens to hundreds of microns) of roots and rhizomes, and some common wetland macrophytes such as *Typha latifolia* (cattail) develop porous tissue that allows enhanced oxygen transport to the roots for respiration (*7*, *8*). Sediment oxygenation may also protect wetland plants from the toxicity of reduced organic compounds, in part via a mechanism of oxidized iron root plaque formation (*7*).

Numerous studies suggest that the predominant Fe root plaque phase is Fe(III) oxyhydroxide, including amorphous ferric oxyhydroxides, goethite (α-FeOOH), and lepidocrocite (γ-FeOOH) (*9*−*11*). However, some have proposed that the plaque includes a mixture of both Fe(II) and Fe(III) solid phases (*12*−*14*). Hansel et al. (*15*, *16*) first used X-ray absorption near-edge spectroscopy (XANES) to determine Fe (and As) speciation in *Phalaris arundinacea* (reed canarygrass) and *Typha latifolia* roots, offering direct evidence that the rhizosphere composition can be highly variable, containing mostly hydrated Fe oxides (e.g. ferrihydrite) but also some crystalline Fe(III) oxides (α- and γ-FeOOH) and Fe(II) carbonate ($FeCO_3$). Further, Weiss et al. (*17*) recently determined that, although the wetland plant rhizosphere environment is a highly active region of Fe(II) oxidation and Fe(III) reduction, the presence of Fe(III) root plaques in many anoxic environments indicate that, on balance, Fe(III) plaques can persist on root surfaces. This Fe(III) plaque, in turn, may provide an important repository for aqueous As in contaminated sediments (*18*).

The high sorptive affinity of As(V) for Fe(III) hydroxides has led researchers to investigate arsenic retention in root plaques (*18*−*20*). Until recent analytical advances, direct evidence of the spatial distribution and speciation of As in Fe plaques was limited. Hansel et al. (*15*, *16*) provided the first X-ray fluorescence (XRF) microtomographic images of As and Fe spatial distributions in wetland plant roots. XRF microtomography, which obtains a micron-scale cross-sectional elemental map through a root without physical slicing, overcomes certain problems presented by other microanalytical techniques, including the need for sample sectioning, which may alter metal distribution by smearing and distort root geometry. A tradeoff is that, given the relatively small masses of metals present in these samples and the number of data points required for cross-sectional reconstruction of each image, data collection is time-consuming, and only a few samples have been studied to date.

The objective of this study was to better characterize the spatial associations and speciation of As in Fe plaques and to gain a better understanding of the potential for plaques to sequester aqueous As. We applied XRF microtomography and XANES to quantify As and Fe elemental concentrations and to determine spatial distributions and oxidation states within *T. latifolia* root plaques in a wetland containing arsenic at levels as high as 1 wt %. These micron-scale analyses were then coupled to chemical extractions to determine if the micron-scale concentrations were representative of the root population. We then extrapolated the findings to assess the potential impact of these common wetland plant roots on sequestering aqueous As in a contaminated wetland.

* Corresponding author phone: (310)829-1441; fax: (310)829-2155; e-mail: nblute@mcguireinc.com.
† Massachusetts Institute of Technology.
‡ Present address: McGuire Environmental Consultants, Inc., Santa Monica, CA.
§ Present address: Wellesley College Department of Geology, Wellesley, MA.
|| Consortium for Advanced Radiation Sources, University of Chicago.
⊥ Department of Geophysical Sciences, University of Chicago.

10.1021/es049448g CCC: $27.50

Published on Web 10/02/2004

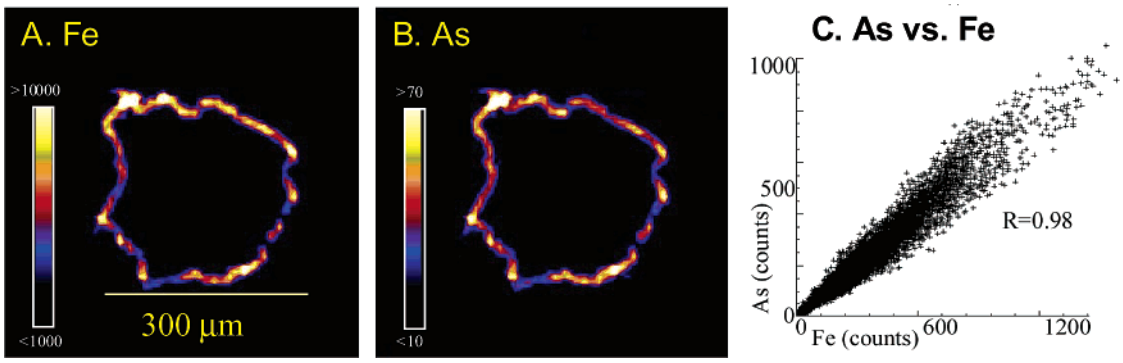

FIGURE 1. XRF microtomographic images of a cross-section through a 300 μm diameter *T. latifolia* root. Higher fluorescence intensities corresponding to higher concentrations are nearer to the hot end of the color spectrum (white then yellow, orange, etc). Color bars show the range of displayed concentrations in μg g^{-1}. Figure 1C plots As versus Fe for the 300 μm root (Figure 1A-B). The correlation between As and Fe for 4 μm-wide analysis locations is high (R = 0.98, 1C), particularly with each data point representing a single 4 μm-wide analysis area.

Materials and Methods

Site Description. The Wells G & H (WGH) wetland is a Superfund site located in Woburn, MA, downstream of the Industri-Plex Superfund site but connected by the Aberjona River. Arsenic in the wetland derives mainly from industrial sources, including historic use of arsenian pyrite in sulfuric acid manufacturing and production of lead arsenate pesticides (*21*, *22*). The WGH wetland is a riverine peatland consisting primarily of emergent macrophytes, notably *Typha latifolia* (cattail).

Root Collection. Fresh *T. latifolia* root samples were obtained from the WGH wetland several days prior to analysis. A 0.027 m^3 block of sediment, containing root material from the zone of greatest root density (0−30 cm), was transferred into a N_2-purged glovebag in the field and transported to the lab for processing the same day. Live roots were hand-separated from the sediment in a N_2-purged glovebag to prevent oxidation of additional ferrous iron on the roots. A portion of the roots was washed with deoxygenated (<0.3 mg O_2 L^{-1}) Milli-Q water, and the rest of the roots were left with adhering sediment.

Microtomography Root Preparation and Analysis. Both freeze-dried and oil-impregnated roots were used for X-ray analysis. In early XRF microtomography tests of elemental distribution, we found that wet roots dried during the required analysis time and lost structural integrity. Freeze-drying allowed us to perform the more time-intensive analyses for elemental distribution mapping. Roots were freeze-dried in a nitrogen-gas purged Corning desiccator (with a −50 °C cold trap and vacuum pump at 0.02 mmHg).

For redox speciation tests and As oxidation state mapping, we subsequently developed a methodology to impregnate fresh roots with oil, both to minimize potential oxidation during freeze-drying and to prevent evaporation-induced shrinkage and distortion of the roots during analysis. To gradually replace the water, roots were first immersed in isopropyl alcohol in a glovebox with a nitrogen gas atmosphere for 24 h. Increasing amounts of mineral oil were added into the alcohol over a 48 h period until most of the solution was oil (due to alcohol evaporation).

Elemental distributions through cross-sections of the roots were determined by XRF microtomography at GeoSoilEnviroCARS beamline 13-ID-C, Advanced Photon Source (APS), Argonne National Laboratory. The APS ring was operated at 7 GeV. The beamline utilized APS Undulator A (158 poles), a Si(111) cryogenic double crystal monochromator that was detuned by approximately 50%, and Kirkpatrick-Baez microfocusing optics (*23*). XRF data were collected simultaneously for several elements using a solid state, multichannel germanium detector and a beam energy of 16.3 keV. For fluorescence tomography and As oxidation state mapping, roots were mounted on a computer-controlled platform, translated at 5−10 μm steps through the stationary 4 μm pencil beam, rotated by 5° around the vertical axis, then repeatedly translated, and rotated up to 180°. Dwell time was one second per step. Tomographic reconstructions were generated by filtered backprojection (*24*). Absorption effects were negligible for the elements of interest. Fe and As plaque concentrations were calculated by comparison with the standard reference material thin film (NIST SRM 1833). Maximum concentrations and averages were calculated using a density estimate of 1 g cm^{-3}. The minimum detection limits for Fe and As were 500 and 3 μg g^{-1}, respectively. An aluminum detector filter was used to suppress the intense Fe K-fluorescence, thus increasing the detection limit for Fe. The As oxidation state map was produced by measuring fluorescence intensities at the As(III) white line energy (11 869.2 eV), at an energy above the edge for total As (12 000 eV), and at an energy below the edge for background.

Bulk Fe and As root oxidation states were determined using a defocused 400 μm beam (width and height), during which we collected 7 spectral scans for Fe and 19 for As (i.e. different due to count rates). Initial and final scans were compared to ensure redox changes did not occur during analysis, then the spectral scans were summed to produce single Fe and As XANES spectra. Arsenic redox speciation calculations were performed using WinXAS v.2.1 software (*25*).

Chemical Extractions of Root Plaques. Sequential extractions of root subsamples (between 2 and 18 g, depending on availability in each increment) were performed to determine if As was adsorbed or coprecipitated. An abbreviated extraction procedure based on the method of Keon et al. (*26*) was used to apportion three As pools: weakly adsorbed (1 M $MgCl_2$, 2 h), strongly adsorbed (1 M NaH_2PO_4, 24 h), and coprecipitated As (with amorphous and crystalline metal oxides, carbonates, or amorphous sulfides; 0.05 M Ti(III)-Cl_3-citrate-EDTA-bicarbonate, 2 h). Aqueous As was measured by graphite furnace atomic absorption spectrometry (Perkin-Elmer 4100ZL) or hydride generation atomic fluorescence (Excalibur).

Extracted Fe and As masses were normalized by wet root masses. Portions of wet roots were dried to obtain a dry root to wet root ratio (approximately 0.15). The quantity of extracted Fe and As per unit volume of sediment was then determined using a value of 11 cm^3 plaque per 27 g of wet root weight ((*27*) the average of multiple cores adjusted for a plaque thickness of 40 μm) and an estimated plaque density of 1 g plaque per cm^3 (for plant material and air spaces mixed with Fe oxyhydroxides).

Results and Discussion

Elemental Distributions in Root Plaques. Typical roots of *T. latifolia* ranged from 100 to 500 μm in diameter, and the XRF microtomographic images indicated that the iron-rich plaques were approximately 40 $\pm$ 10 μm thick ($n = 3$). The plaque contained As throughout, and As was highly spatially correlated with Fe (R = 0.98 at the resolution of 4 μm; Figure 1a−c). This high correlation of As with Fe, and the observation of little As in the interior of the roots tested, contrasts with findings by Hansel et al. (*16*) for *P. arundinacea* roots. The difference may arise from interspecies differences in As uptake or speciation of As in the contamination source. *T. latifolia* roots growing in WGH wetland sediments sequestered more As at plaque locations containing higher Fe concentrations (as observed in Figure 1), suggesting that the plaque Fe directly affects the capacity for As in this environment.

Iron concentrations in the plaque of two roots studied by XRF microtomography were 0.03 and 0.8 g Fe g^{-1} wet plaque. Sequential extractions of a much larger sample size (2−18 g of roots) yielded Fe levels of 0.04 to 0.16 g Fe g^{-1} wet plaque. Measured As plaque concentrations on the same subsamples ranged from 30 to 200 μg As g^{-1} wet plaque by XRF microtomography and 260−1200 μg As g^{-1} wet plaque by sequential extractions. The difference observed for As concentrations determined by extractions and microtomography likely arises from interplaque variability and significant variation in analytical volume, spanning nearly 7 orders of magnitude (from between 1 and 7 cm^3 of plaque analyzed by extractions and 2×10^{-7} cm^3 analyzed by microtomography).

The XRF microtomographic and sequential extraction findings taken together suggest that the limited microtomographic data may be representative of the larger root population. Further, the concentrations measured by both of these methods are very similar to plaque Fe concentrations reported recently by Weiss et al. (*17*) for *T. latifolia* plaque and by Otte et al. (*19*) for salt marsh plants *Halimiome portulacoides* (sea purslane) and *Spartina anglica* (cordgrass)-plaques. Weiss et al. (*17*) report Fe plaque concentrations up to 900 μmol Fe g^{-1} dry weight root. Otte et al. (*19*) found similar Fe concentrations of approximately 500 μmol Fe g^{-1} dry weight root in both species tested. This range corresponds to approximately 0.01 to 0.02 g Fe g^{-1} wet plaque when normalized with the factor used for our calculations to convert dry root weight to wet plaque (see Methods).

We also compared As concentrations determined in *Halimione portulacoides* rhizosphere concretions by Caetano and Vale (*18*) with our findings, although the formation of concretions is more extensive than root plaques due to higher rates of radial oxygen loss and dense root structures (i.e. concretions extending to approximately 4 mm thickness compared to 40 μm thickness for plaques). Caetano and Vale (*18*) reported concentrations of 3.1 μmol As g^{-1} dry concretion, which corresponds to 230 μg As g^{-1} dry concretion. Therefore, the plaque concentrations of Fe in all three wetland plant species and As in *H. portulacoides* are within the same order of magnitude as our findings by XRF microtomography and extractions.

Fe and As concentrations determined in our study yield molar As-to-Fe ratios of 7 and 20 mmol As per mol Fe from microtomography results and 40 mmol As per mol Fe by sequential extractions. Greater than 90% of the extracted As was extractable by orthophosphate, indicating that the As is likely immobilized by surface adsorption rather than by coprecipitation in iron phases. The As-to-Fe ratio is within the range expected for As adsorbed on hydrated ferric oxides, which can exceed 40 mmol per mol Fe *(28)*.

Redox Speciation of Fe and As in Root Plaque. Iron XANES (Figure 2) of *T. latifolia* roots and model compounds demonstrated that the plaque was predominantly Fe(III) (based on the close match in spectral energy and shape with the spectra for pure Fe(III) compounds). The detection limit of Fe(II) by this XANES analysis was approximately 5%.

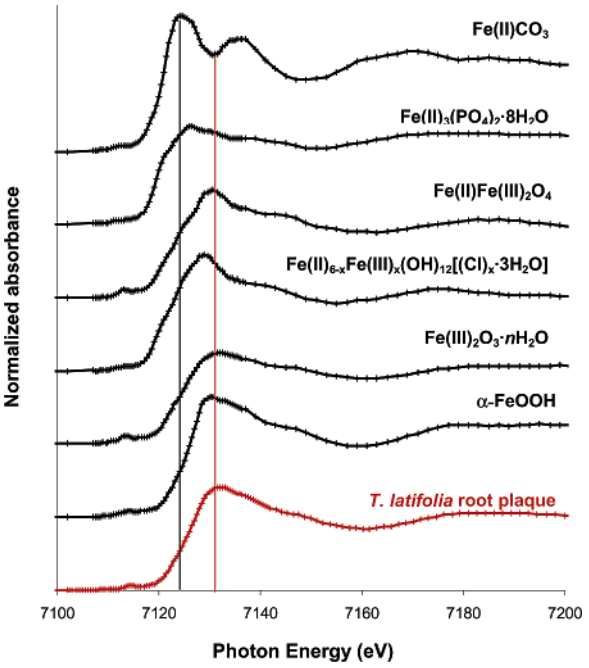

FIGURE 2. Average Fe oxidation state of a root cross-section. Iron K-edge XANES summed spectrum ($n = 7$) through the same 300 μm root imaged in Figure 1 (different spot). XANES spectra for model compounds are shown, including siderite ($FeCO_3$), vivianite ($FePO_4$), green rust ($Fe_{6x}(II)Fe_x(III)(OH)_{12}[(Cl)_x \cdot 3H_2O]$), magnetite ($Fe(II)Fe(III)_2O_4$), ferrihydrite ($Fe_2O_3 \cdot nH_2O$), and goethite (α-FeOOH). (Iron compound spectra were provided by C. Hansel, Stanford University). The two vertical lines show the approximate white line energies for Fe(II) and Fe(III), respectively, along the *x*-axis. The plaque spectrum is more consistent with those of the Fe(III) model compounds than mixed Fe(III)-Fe(II) or Fe(II) compounds.

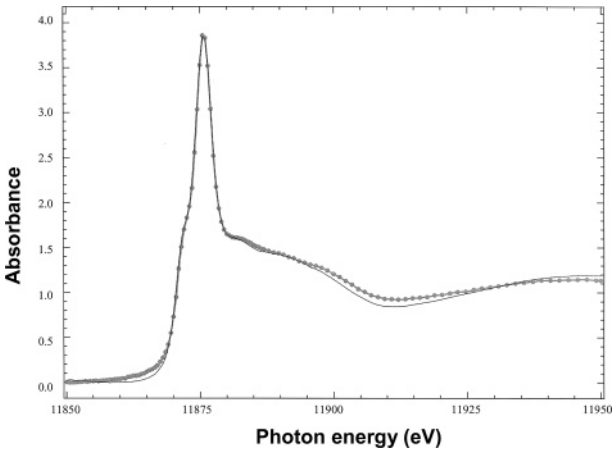

FIGURE 3. Average As oxidation state of a root cross-section. Arsenic K-edge XANES summed spectrum (n = 19 scans) for a 300 μm diameter root cross-section. Circles are data points; the solid line is the data curve fit using As(III) and As(V) on α−FeOOH as model compounds. The curve fit showed that the plaque is comprised of approximately 20% As(III) and 80% As(V).

XANES redox speciation of As in two root sections yielded an average of 20% As(III) (Figure 3). Interestingly, the bulk speciation of *T. latifolia* roots by Hansel et al. (*16)* yielded a very similar proportion of As(III) (18%) with their XANES fits and predominately adsorbed As, which is in agreement with our sequential extraction results.

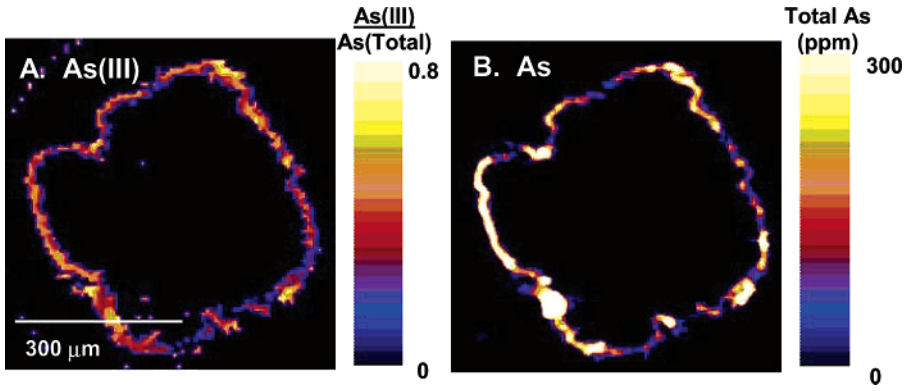

FIGURE 4. Arsenic oxidation state map for root plaque. (A) The color bar reflects the proportion of As(III) compared to total As. (B) The total As image (in μg g^{-1}) is also shown with associated color bar. The As(III) distribution is heterogeneous with no observed systematic radial gradients.

Arsenic oxidation state microtomograms (Figure 4) showed that As(III) and As(V) were distributed heterogeneously in the root plaque, with little evidence for systematic gradients as might be hypothesized due to a radial oxygen fugacity gradient from the roots. The coexistence of As(III) and As(V) suggests that both oxidation states can be immobilized in Fe root plaques. Arsenic porewater speciation in the root zone (0−30 cm depth) of this wetland, which is the presumed source of As in the plaque, averaged 50% ± 25% As(III) (*27*). Oxidation of As(III) in the rhizosphere, relative uncertainties in the XANES analysis due to a low number of root section analyses, porewater variation in the As(III):As(V) ratio during plaque formation, or a lesser adsorptive affinity of As(III) could all be responsible for the lower measured percentage of As(III) relative to As(V) in the plaque, as compared with porewater.

Implications of Root Plaque for Sequestering Porewater Arsenic. The total amount of As sequestered in root plaque is significant relative to the mass of dissolved As in the root zone of the wetland. The concentration of dissolved As typically ranged from 0.30 to 0.77 mg As L^{-1}. The concentration of As in the porewater that would be produced if the As stored in the root plaques were released was estimated by multiplying the average plaque As concentration by plaque volume per unit volume of sediment and by the plaque density, and then dividing by porosity (see Methods). The resulting porewater concentration would be 7 to 44 mg As L^{-1}, up to 50 times higher than ambient porewater in WGH wetland (in the absence of possible As redistribution into other solid phases).

The approximately 40 μm thick Fe(III)-containing plaques that encircle *T. latifolia* roots are thus significant for their sequestration of both As(III) and As(V) from porewater. Because the aqueous geochemical conditions at the WGH site are typical of wetland environments, we suggest that similar root plaques formed by wetland plants are likely to play a significant role in arsenic cycling in other contaminated settings. Further, *T. latifolia* plaque may become reduced and hence solubilized, for example in the event of vegetation loss or possibly during winter senescence (*17*). Ecosystem alterations that affect the redox environment of the rhizosphere in wetland sediments, resulting in the reduction of Fe(III) plaques, could significantly increase aqueous arsenic concentrations.

Acknowledgments

We thank C. H. Swartz and J. A. Jay for field and laboratory assistance, C. Hansel for generously providing XANES spectra of model compounds, and the work of three reviewers. This study was supported by the EPA NCERQA STAR Fellowship Program and the National Institute of Environmental Health Sciences (NIEHS) Superfund Basic Research Program Grant 5P42ES04675-06. Use of the Advanced Photon Source was supported by the U.S. Department of Energy, Office of Science, Office of Basic Energy Sciences, under Contract No. W-31-109-Eng-38. The GeoSoilEnviroCARS beamline is supported by the National Science Foundation, the Department of Energy, and the State of Illinois.

Literature Cited

(1) Oremland, R. S.; Stolz, J. F. *Science* **2003**, *300*, 939−944.
(2) Harvey, C. F.; Swartz, C. H.; Badruzzaman, A. B. M.; Keon-Blute, N.; Yu, W.; Ali, M. A.; Jay, J.; Beckie, R.; Niedan, V.; Brabander, D.; Oates, P. M.; Ashfaque, K. N.; Islam, S.; Hemond, H. F.; Ahmed, M. F. *Science* **2002**, *298*, 1602−1606.
(3) Nordstrom, D. K. *Science* **2002**, *296*, 2143-2145.
(4) Ma, L. Q.; Komar, K. M.; Tu, C.; Zhang, W.; Cai, Y.; Kennelley, E. D. *Nature* **2001**, *409*, 579.
(5) Smedley, P.; Kinniburgh, D. *Appl. Geochem.* **2002**, *17*, 517−568.
(6) Mitsch, W. J.; Gosselink, G. *Wetlands*, 2nd ed.; Van Nostrand Reinhold: New York, 1993.
(7) Armstrong, W. *Adv. Bot. Res.* **1979**, *7*, 226−332.
(8) Kludze, H. K.; DeLaune, R. D. *Soil Sci. Soc. Am. J.* **1996**, *60*, 616−621.
(9) Bacha, R.; Hossner, L. *Soil Sci. Soc. Am. J.* **1977**, *41*, 931−935.
(10) Chen, C. C.; Dixon, J. B.; Turner, F. T. *Soil Sci. Soc. Am. J.* **1980**, *44*, 1113−1119.
(11) Taylor, G. J.; Crowder, A. A. *Am. J. Bot.* **1984**, *71*, 666−675.
(12) St-Cyr, L.; Crowder, A. *J. Plant Nutr.* **1988**, *11*, 1253−1261.
(13) Wang, T.; Peverly, J. H. *Soil Sci. Am. J.* **1996**, *60*, 323−329.
(14) Wang, T.; Peverly, J. *Soil Sci. Soc. Am. J.* **1999**, *63*, 247−252.
(15) Hansel, C. M.; Fendorf, S. *Environ. Sci. Technol.* **2001**, *35*, 3863−3868.
(16) Hansel, C.; LaForce, M.; Fendorf, S.; Sutton, S. *Environ. Sci. Technol.* **2002**, *36*, 1988−1994.
(17) Weiss, J. V.; Emerson, D.; Megonigal, J. P. *FEMS Microbiol. Ecol.* **2004**, *48*, 89−100.
(18) Caetano, M.; Vale, C. *Mar. Chem.* **2002**, *79*, 261−271.
(19) Otte, M. L.; Kearns, C. C.; Doyle, M. O. *Bull. Environ. Contam. Toxicol.* **1995**, *55*, 154−161.
(20) Doyle, M. O.; Otte, M. L. *Environ. Pollut.* **1997**, *96*, 1−11.
(21) Aurilio, A.; Durant, J. L.; Hemond, H. F.; Knox, M. L. *Water, Air, Soil Pollut.* **1995**, *81*, 265−282.
(22) Brabander, D.; Keon, N.; Stanley, R.; Hemond, H. F. *PNAS* **1999**, *96*, 14635−14640.
(23) Eng, P.; Newville, M.; Rivers, M.; Sutton, S. *SPIE Proc* **1998**, *3449*, 145.
(24) Rivers, M.; Sutton, S.; Eng, P. *Developments in X-ray Tomography II, SPIE Proc.* **1999**, *3772*, 78−86.
(25) Ressler, T. WinXAS v. 2.1, *J. Synchrotron Radiat.* **1998**, *5*, 118.
(26) Keon, N. E.; Swartz, C. H.; Brabander, D. J.; Harvey, C.; Hemond, H. F. *Environ. Sci. Technol.* **2001**, *35*, 2778−2784.
(27) Keon, N. Ph.D. Dissertation, Massachusetts Institute of Technology, 2002.
(28) Fuller, C. C.; Davis, J. A.; Waychunas, G. A. *Geochim. Cosmochim. Acta* **1993**, *57*, 2271−2282.

Received for review April 12, 2004. Revised manuscript received August 2, 2004. Accepted August 19, 2004.

ES049448G